ABSTRACT

We report *Chandra* observations of **14 high-redshift (z=4.06–5.27), optically selected quasars**. **10** of these quasars are **detected**, thus increasing the number of $z > 4$ X–ray detected quasars from 15 to 25 ($\approx 67\%$). Our detections, obtained with an average exposure time of ≈ 4.1 ks, include **four of the five highest-redshift X–ray detected quasars** to date, among them SDSSp J021043.17−001818.4 which, at $z = 4.77$, represents the highest-redshift radio-loud quasar ever detected in the X–ray band. Among the 4 undetected quasars we find two Broad Absorption Line quasars and one weak emission-line quasar. Comparing the *Chandra* quasars' spectral energy distributions (SEDs) with those of lower-redshift samples indicates that the *Chandra* quasars are X–ray fainter by a factor of ≈ 2. This **X–ray faintness** could be associated with the presence of **large amounts of gas in the primeval galaxies** harboring these quasars, as suggested by recent studies at other wavelengths, or due to **"trapping radius" effects**.

OVERVIEW

In the last few years, high-z quasars have been a subject of renewed interest primarily thanks to the outstanding discoveries coming from the **Sloan Digital Sky Survey** (**SDSS**; York et al. 2000). About 1000 $z > 4$ quasars are expected over the next five years, ≈ 100 of which should be at $z > 5$ (e.g., Schneider 1999). $z > 4$ quasars can allow one to:

- **Investigate the formation of galaxies and the large-scale structures** in the early Universe. From the Eddington limit, luminous quasars are expected to host $\approx 10^{8-9}$ $M_\odot$ black holes, which are likely to be associated with the rare high peaks in the primordial density field;
- **Probe the gas metallicity** through quasar emission-line strengths, and hence possibly constrain **the star-formation history and the chemical enrichment processes of primordial environments** (e.g., Hamann & Ferland 1999);

Although $z > 4$ quasars have been extensively studied from the millimeter to the optical, little was known about their X–ray properties until the advent of *Chandra*. The most systematic pre-*Chandra* X–ray study of $z > 4$ quasars was carried out by Kaspi, Brandt, & Schneider (2000; hereafter KBS) using archival *ROSAT* data. While the most basic X–ray properties of

$z > 4$ quasars appeared to be consistent with those of lower-redshift samples, the constraints on their X–ray spectral shapes were weak. At present, a spectral analysis has been possible for only 4 objects: they are blazars, whose X–ray spectral and variability properties are probably jet-induced (e.g., Fabian et al. 2001).

X–ray studies of high-z quasars can probe:

- **Any possible evolution in the continuum shapes of quasars** (e.g., Vignali et al. 1999);
- **The environments of high-z quasars**; i.e. the presence of **X–ray absorption**, which to date has been detected in many high-z radio-loud quasars (e.g., Elvis et al. 1994; Cappi et al. 1997) and perhaps in some radio-quiet quasars at $z \approx 2$ (e.g., Reeves & Turner 2000);
- **How massive black holes are being fed**, and the presence of disk instabilities, "trapping radius" effects (e.g., Begelman 1978) or other energetically important phenomena;
- **The role of high-z quasars in heating the intergalactic medium (IGM)**.

Although X–rays alone generally do not produce a fully ionized IGM, the primary and secondary ionizations created by X–rays can give rise to a mild increase in temperature and partial reionization (e.g., Shull & van Steenberg 1985; Venkatesan, Giroux, & Shull 2001).

PROJECT GOALS

We have started a project to measure the X–ray properties of the most distant quasars, primarily those found by the SDSS, using the new generation of X–ray observatories. **The SDSS multicolor selection method provides a sample of quasars that has been consistently selected in a well-defined manner.** In this regard, SDSSp J104433.04–012502.2 at $z = 5.72$ (Fan et al. 2000b) has been successfully detected by *XMM-Newton* (Brandt et al. 2001; hereafter B01) with a surprisingly low X–ray flux. The **main goals** of this work are **to investigate whether the highest-redshift quasars show different X–ray properties than do local quasars, and to put the results into a comprehensive picture which links these objects to the growth of massive black holes from the first collapsed structures at the end of the cosmic "dark age."** *Chandra* is ideal for this program, given its sub-arcsec angular resolution coupled with an extremely low background; this combination efficiently allows detection of very faint point sources with relatively low exposure times.

X–ray Detections

The present sample consists of **14 high-redshift optically selected quasars** observed by *Chandra* with ACIS (CCD S3) during Cycles 1 and 2 (see **Table 1**). SDSS 0210−0018 was serendipitously discovered in the field of the quasar SDSS 0211−0009 and, at $z = 4.77$, represents the highest-redshift X–ray detected radio-loud quasar (RLQ) to date. All of the remaining quasars are radio-quiet (RQQs). Nine objects have been successfully detected with WAVDETECT using a false-positive threshold of 10^{-6}. Two X–ray photons were found within $0.8''$ of the optical position of SDSS 1208+0010 ($z = 5.27$). The Poisson probability of obtaining two counts or more when 0.0211 counts are expected from the background is $\approx 2.2 \times 10^{-4}$. Extensive Monte-Carlo simulations have confirmed the validity of the Poisson approximation for the SDSS 1208+0010 field (see Vignali et al. 2001); therefore this source also has to be considered detected by *Chandra* (at the 3.9σ confidence level), thus increasing the **number of** *Chandra* X–ray detected $z > 4$ quasars to **10**.

Chandra adaptively smoothed (when possible) images of the quasars in the 0.5–8 keV band are shown in **Fig. 1**. The source photometry results are reported in **Table 2** in four energy bands, covering the rest-frame energy range 1.7–45 keV at the average $z \approx 4.6$ of this sample, while the optical/X–ray properties are reported in **Table 3**.

While SDSS 0210−0018, PSS 1057+4555 and PC 1247+3406 have band ratios (BR, i.e. the ratio between the 2–8 keV and 0.5–2 keV counts) consistent with unabsorbed $\Gamma \approx 2$ power-law spectra,

PSS 0248+1802 (BR=$0.67^{+0.51}_{-0.34}$) is likely to be **absorbed by $N_H > 5 \times 10^{23}$ cm^{-2}**. Given the source's 0.3–0.5 keV X–ray counts, a complex absorber is likely.

X–ray Non-Detections

Four sources were not detected: the Broad Absorption Line quasars (BALQSOs) SDSS 1129−0142 ($z = 4.85$) and SDSS 1605−0112 ($z = 4.92$), the quasar with no optical lines SDSS 1532−0039 ($z = 4.62$; Fan et al. 1999b, 2000a), and the quasar PSS 1435+3057 ($z = 4.35$). X–ray studies at low redshift show that absorption plays a major role in hiding BALQSOs in the X–ray band (e.g., Green & Mathur 1996; Gallagher et al. 1999), with typical N_H of $\approx$ (1–10)$\times 10^{22}$ cm^{-2} (high-ionization BALQSOs) to $\gtrsim 5\times 10^{23}$ cm^{-2}(low-ionization BALQSOs; e.g., Green et al. 2001). The *Chandra* non-detections of the two BALQSOs, coupled with their α_{ox} upper limits of −1.88 and −1.82, respectively (see **Table 3**), make them good candidates to be highly-absorbed objects, perhaps being Compton thick. Assuming the average α_{ox} of the sample without the BALQSOs (−1.75) and $\Gamma = 2.0$, we infer $N_H \gtrsim 5 \times 10^{23}$ cm^{-2} for both sources. It is notable that SDSS 1044−0125 (B01), SDSS 1129−0142 and SDSS 1605−0112 all appear to have large X–ray absorbing column densities more characteristic of those seen in low-ionization BALQSOs at low redshift. Since it is unlikely a priori that all three of these objects are low-ionization BALQSOs (assuming, as at low redshift, that only $\sim 1/10$ of BALQSOs are low-ionization BALQSOs), **this may suggest that the X–ray absorption in high-ionization BALQSOs increases with redshift**.

RESULTS

- **10 new $z > 4$ X–ray detected quasars** (67% increase) — see **Fig. 2**
- ***Chandra* quasars tend to be X–ray faint** — see **Table 3** and **Fig. 3**

$\Longrightarrow$ SDSS is more effective at finding quasars with X–ray absorption or weaker X–ray SEDs ?

- Comparison with lower-redshift samples of optically selected quasars — see **Fig. 4**

$\Longrightarrow$ ***Chandra* quasars have lower $\alpha_{\rm ox}$ values**

$z < 0.5$ BQS RQQs: $\langle\alpha_{\rm ox}\rangle = -1.56\pm0.02$

ROSAT RQQs (KBS): $\langle\alpha_{\rm ox}\rangle = -1.58\pm0.03$

***Chandra* RQQs:** $\langle\alpha_{\rm ox}\rangle = \mathbf{-1.78}\pm0.03$ (-1.75 ± 0.03 without the two undetected BALQSOs)

The postulated steepening of $\alpha_{\rm ox}$ with increasing optical luminosity (e.g., Avni, Worrall, & Morgan 1995) cannot explain this result easily, since the SDSS objects have lower optical luminosities on average than the KBS sample.

- **No clear evidence for a systematic decrease of $\alpha_{\rm ox}$ with redshift in the range $z \approx 4$–6** — see **Fig. 5**, but further investigations at the highest redshifts are required

21 more quasars coming over the next year

• **X–ray faintness** possibly due to **(a)** **absorption by molecular gas** which is likely to be present in high-z quasars (e.g., Omont et al. 2001, and references therein) or **(b)** **"trapping radius" effects** (i.e., X–rays are dragged back into the black hole; e.g., Begelman 1978).

X–rays from the Dawn of the Modern Universe: the Future

• ***Chandra*** **and** ***XMM-Newton*** **as starting points for future high-redshift X–ray efforts with** ***Constellation-X*** **and** ***XEUS***

$\Longrightarrow$ **Detailed X–ray spectroscopic studies of the postulated evolution of the X–ray continua and absorption with redshift**

$\Longrightarrow$ **Further constraints on the fueling processes in massive black holes during their growth phase**

Table 1: *Chandra* Observation Log

ID #	Object Name	z	$\Delta_{\rm Opt-X}$ (arcsec)	Exp. Time (ks)	Ref.
1	**SDSSp J021043.17−001818.4**	**4.77**	0.6	4.95	(1)
2	**SDSSp J021102.72−000910.3**	**4.90**	0.3	4.95	(2)
3	**BRI 0241−0146**[a]	**4.06**	0.2	7.37	(3)
4	**PSS 0248+1802**[a]	**4.43**	0.7	1.73	(4)
5	**BRI 1033−0327**[a]	**4.51**	0.9	3.45	(3)
6	**PSS 1057+4555**[a]	**4.10**	0.8	2.81	(5)
7	**SDSSp J112956.10−014212.4**	**4.85**	...	4.88	(6)
8	**SDSSp J120823.82+001027.7**	**5.27**	0.6	4.68	(6)
9	**PC 1247+3406**	**4.90**	0.9	4.68	(7)
10	**PSS 1317+3531**[a]	**4.36**	0.3	3.97	(5)
11	**PSS 1435+3057**[a]	**4.35**	...	2.81	(4)
12	**PSS 1443+2724**[a]	**4.42**	0.5	2.17	(4)
13	**SDSSp J153259.96−003944.1**	**4.62**	...	5.15	(8–9)
14	**SDSSp J160501.21−011220.0**	**4.92**	...	4.64	(9)

NOTE. — [a] *Chandra* archival observation.

REFERENCES. — (1) Fan et al. 2001; (2) Fan et al. 1999a; (3) Storrie-Lombardi et al. 1996; (4) Kennefick et al. 1995; (5) Kennefick, Djorgovski, & de Carvalho 1995; (6) Zheng et al. 2000; (7) Schneider, Schmidt, & Gunn 1991; (8) Fan et al. 1999b; (9) Fan et al. 2000a.

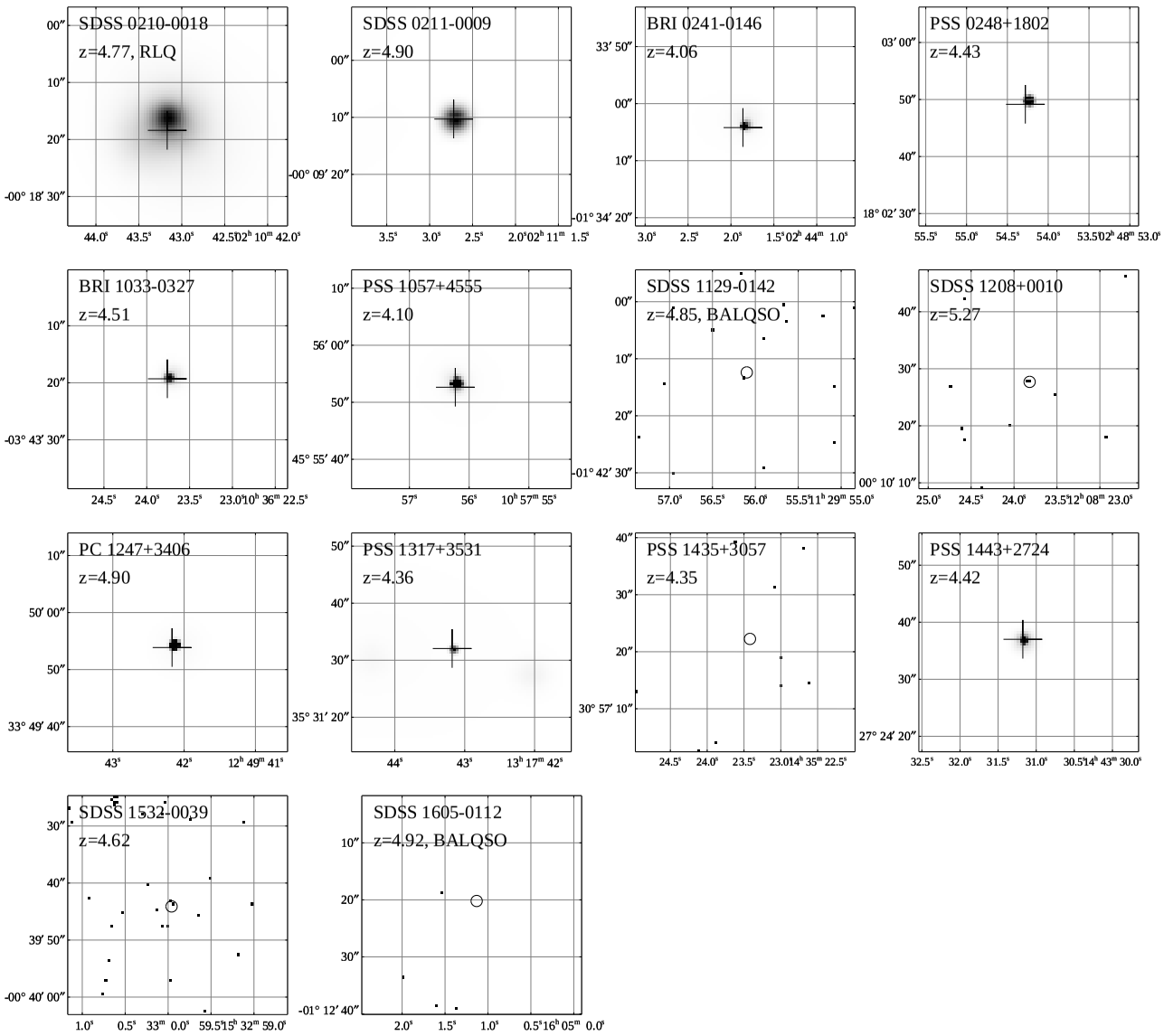

Fig. 1: *Chandra* full-band images of the 14 high-z quasars. A 2σ level of smoothing has been applied for the nine sources with the best statistics. The optical position is indicated either by a cross or by a circle of $1''$ radius.

Table 2: X–ray Counts in Four Energy Bands

Object	[0.3–0.5 keV]	[0.5–2 keV]	[2–8 keV]	[0.5–8 keV]
SDSS 0210−0018	< 3.0	$28.0^{+7.0}_{-5.5}$	$7.6^{+4.5}_{-3.0}$	$35.8^{+7.8}_{-6.5}$
SDSS 0211−0009	< 3.0	$5.0^{+3.4}_{-2.2}$	< 3.0	$5.0^{+3.4}_{-2.2}$
BRI 0241−0146	< 6.4	$9.0^{+4.1}_{-2.9}$	< 7.9	$11.9^{+4.6}_{-3.4}$
PSS 0248+1802	$4.0^{+3.2}_{-1.9}$	$9.0^{+4.1}_{-2.9}$	$6.0^{+3.6}_{-2.4}$	$15.0^{+5.0}_{-3.8}$
BRI 1033−0327	$5.0^{+3.4}_{-2.2}$	$8.0^{+4.0}_{-2.8}$	< 6.4	$9.9^{+4.3}_{-3.1}$
PSS 1057+4555	$6.0^{+3.6}_{-2.4}$	$21.0^{+5.7}_{-4.5}$	$6.0^{+3.6}_{-2.4}$	$26.9^{+6.3}_{-5.2}$
SDSS 1129−0142	< 3.0	< 3.0	< 3.0	< 3.0
SDSS 1208+0010	< 3.0	< 4.8	< 4.8	$2.0^{+2.6}_{-1.3}$
PC 1247+3406	< 4.8	$14.0^{+4.8}_{-3.7}$	$3.0^{+2.9}_{-1.6}$	$18.0^{+5.3}_{-4.2}$
PSS 1317+3531	< 4.8	$3.0^{+2.9}_{-1.6}$	< 3.0	$3.9^{+3.1}_{-1.9}$
PSS 1435+3057	< 3.0	< 3.0	< 3.0	< 3.0
PSS 1443+2724	< 3.0	$7.0^{+3.8}_{-3.6}$	< 7.9	$10.0^{+4.3}_{-3.1}$
SDSS 1532−0039	< 3.0	< 3.0	< 6.4	< 6.4
SDSS 1605−0112	< 3.0	< 3.0	< 3.0	< 3.0

NOTE. — Errors on the X–ray counts were computed according to Gehrels (1986). The upper limits are at the 95% confidence level and were computed according to Kraft et al. (1991).

Table 3: Properties of *Chandra* $z > 4$ Quasars

Object	$AB_{1450(1+z)}$	$\log(\nu L_\nu)_{2500}$ [a] [erg s^{-1}]	M_B [a,b]	Count rate [10^{-3} ct/s]	$f_{0.5-2\ keV}$ [c] [10^{-15} cgs]	$\log(\nu L_\nu)_{2keV}$ [b,c] [erg s^{-1}]	α_{ox} [d]
SDSS 0210−0018	19.3	46.3	−26.8	5.65	$28.1^{+8.1}_{-6.0}$	45.3	-1.40 ± 0.07
SDSS 0211−0009	20.0	46.1	−26.2	1.01	$3.1^{+2.2}_{-1.4}$	44.4	$-1.66^{+0.11}_{-0.12}$
BRI 0241−0146	18.4	46.6	−27.5	1.22	$3.8^{+1.9}_{-1.2}$	44.3	$-1.89^{+0.09}_{-0.08}$
PSS 0248+1802	18.1	46.8	−27.9	5.20	$19.6^{+9.0}_{-6.3}$	45.1	$-1.65^{+0.09}_{-0.08}$
BRI 1033−0327	18.8	46.5	−27.2	2.32	$7.6^{+3.9}_{-2.7}$	44.7	-1.70 ± 0.09
PSS 1057+4555	17.6	46.9	−28.3	7.48	$21.6^{+6.5}_{-4.9}$	45.0	-1.72 ± 0.07
SDSS 1129−0142	19.2	46.4	−26.9	<0.61	<1.6	<44.1	<−1.88
SDSS 1208+0010	20.5	45.9	−25.8	0.43	$1.1^{+1.5}_{-0.7}$	44.0	$-1.74^{+0.16}_{-0.18}$
PC 1247+3406	19.2	46.4	−26.9	2.99	$8.7^{+3.2}_{-2.4}$	44.8	-1.61 ± 0.08
PSS 1317+3531	18.9	46.4	−27.1	0.76	$2.2^{+2.2}_{-1.2}$	44.1	$-1.90^{+0.13}_{-0.14}$
PSS 1435+3057	19.1	46.4	−26.9	<1.07	<2.7	<44.2	<−1.83
PSS 1443+2724	19.0	46.4	−27.0	3.22	$9.7^{+5.5}_{-5.1}$	44.8	$-1.63^{+0.10}_{-0.14}$
SDSS 1532−0039	19.4	46.3	−26.7	<1.24	<3.4	<44.4	<−1.74
SDSS 1605−0112	19.4	46.3	−26.8	<0.65	<2.0	<1.77	<−1.82

NOTE:

[a] Computed from the $AB_{1450(1+z)}$ magnitude assuming an optical power-law slope with $\alpha=-0.79$ ($S_\nu \propto \nu^\alpha$).

[b] Computed assuming $H_0=70$ km s^{-1} Mpc^{-1}, $q_0=0.5$ and $\Lambda=0$.

[c] Computed from the count rate assuming a power-law model with $\Gamma = 2.0$.

[d] $\alpha_{ox} = \frac{\log[(f_\nu(2\,\mathrm{keV})/f_\nu(2500\,\text{Å})]}{\log[\nu(2\,\mathrm{keV})/\nu(2500\,\text{Å})]}$

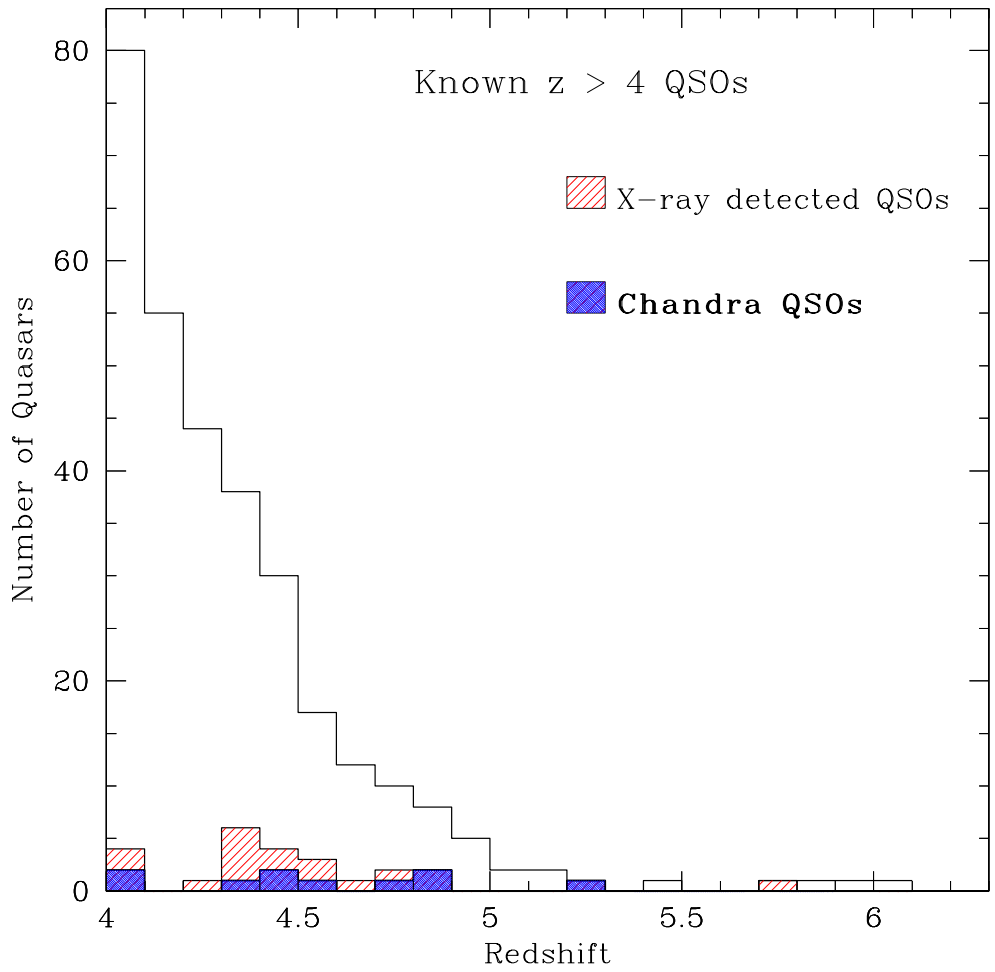

Fig. 2 : Redshift distribution of all known $z > 4$ quasars. The red shaded regions indicate the quasars detected in the X–ray band, and the blue shaded regions show the $z > 4$ *Chandra* detections.

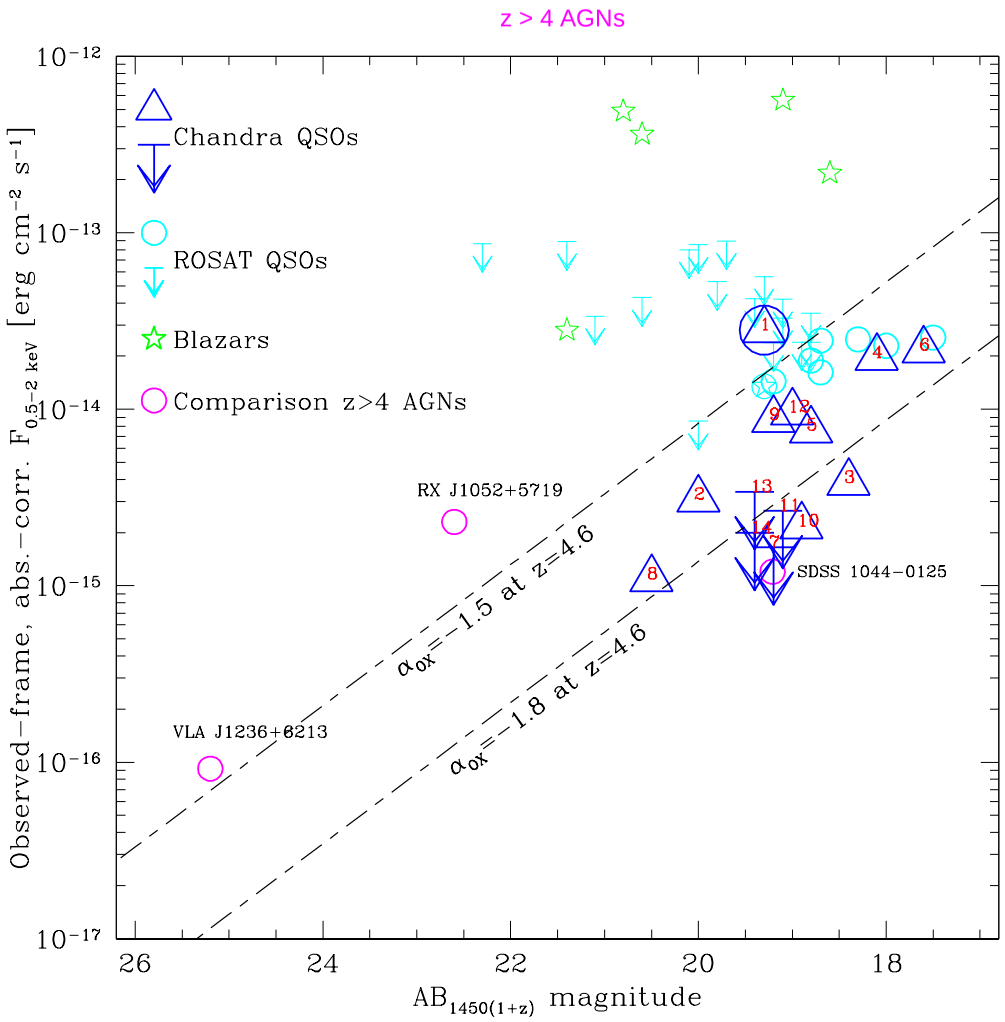

Fig. 3 : Observed-frame, Galactic absorption-corrected 0.5–2 keV flux versus $AB_{1450(1+z)}$ magnitude for $z > 4$ AGNs. Some $z > 4$ AGNs are shown for comparison (details in Vignali et al. 2001). The slanted lines show $\alpha_{ox} = -1.5$ and $\alpha_{ox} = -1.8$ loci for $z = 4.6$ (the average redshift of the present sample).

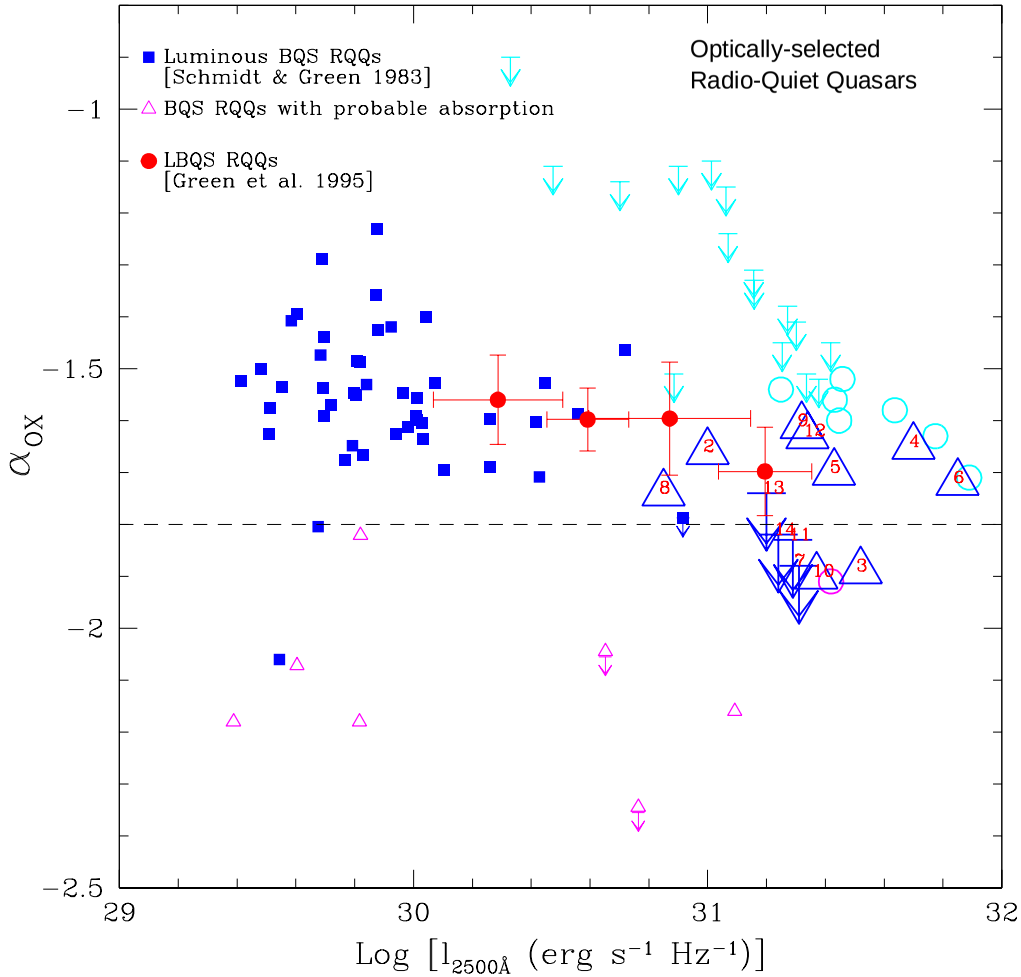

Fig. 4 : α_{ox} versus luminosity density at 2500 Å for optically selected RQQs. As comparison lower-z samples we chose the Bright Quasar Survey (BQS) RQQs (Schmidt et al. 1983) and the Large Bright Quasar Survey (Hewett, Foltz, & Chaffee 1995; stacking analysis results from Green et al. 1995.)

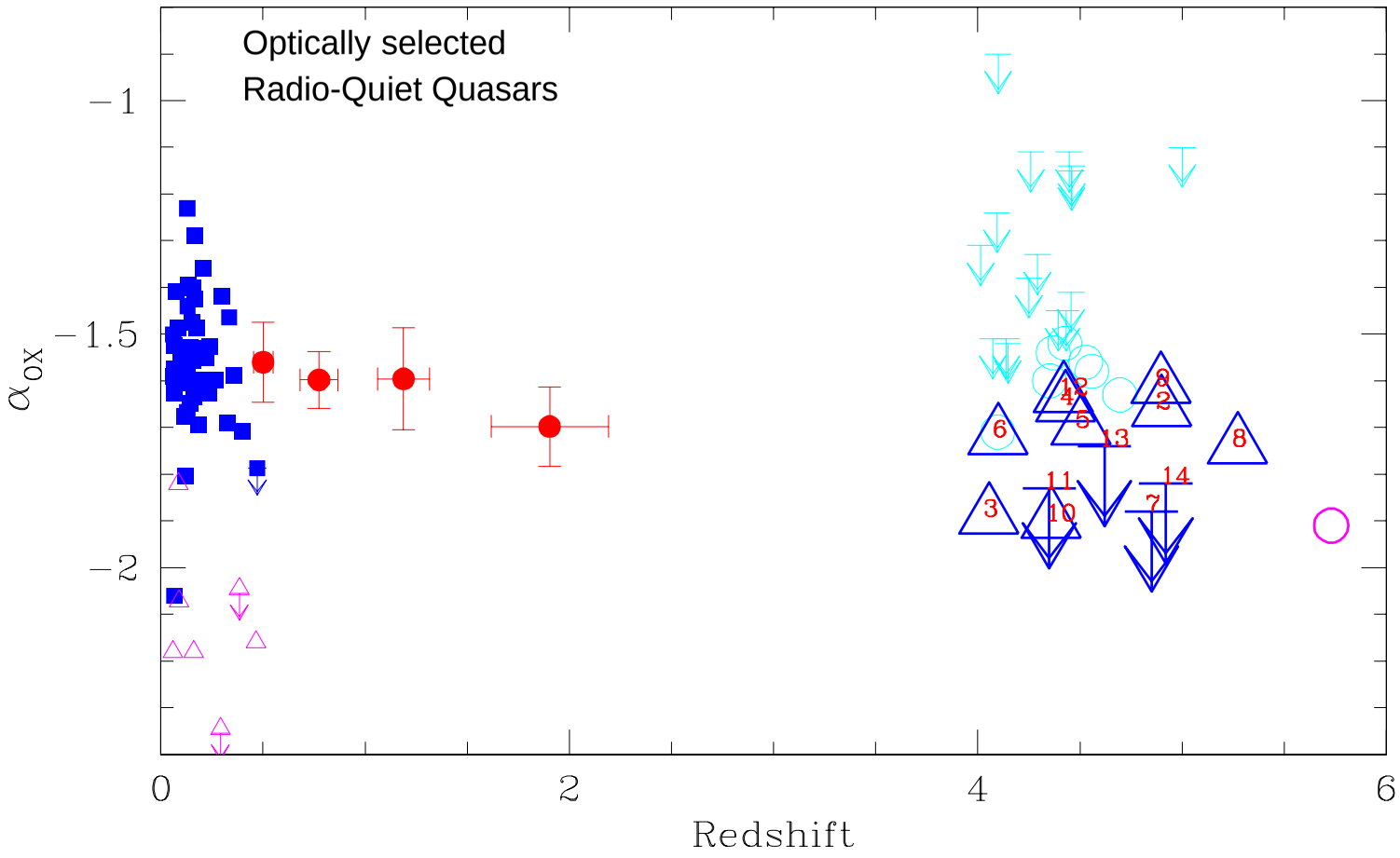

Fig. 5 : α_{ox} versus redshift for samples of optically selected RQQs. For comparison, low-redshift RQQs are also plotted (see previous figure). There is no clear evidence for a systematic decrease of α_{ox} with increasing redshift for $4 < z < 6$. Symbols are as in the previous figures.

References

- Avni, Y., Worrall, D. M., & Morgan Jr., W. A. 1995, *Ap.J.* **454**, 673
- Begelman, M. C. 1978, *M.N.R.A.S.* **184**, 53
- Brandt, W. N., Guainazzi, M., Kaspi, S., Fan, X., Schneider, D. P., Strauss, M. A., Clavel, J., & Gunn, J. E. 2001, *A.J.* **121**, 591 [B01]
- Cappi, M., Matsuoka, M., Comastri, A., Brinkmann, W., Elvis, M., Palumbo, G. G. C., & Vignali, C. 1997, *Ap.J.* **478**, 492
- Elvis, M., et al. 1994, *Ap.J.* **422**, 60
- Fabian, A. C., Celotti, A., Iwasawa, K., McMahon, R. G., Carilli, C. L., Brandt, W. N., Ghisellini, G., & Hook, I. M. 2001, *M.N.R.A.S.* **323**, 373
- Fan, X., et al. 1999a, *A.J.* **118**, 1
- Fan, X., et al. 1999b, *Ap.J.* **526**, L57
- Fan, X., et al. 2000a, *A.J.* **119**, 1
- Fan, X., et al. 2000b, *A.J.* **120**, 1167
- Fan, X., et al. 2001, *A.J.* **121**, 31
- Gallagher, S. C., Brandt, W. N., Sambruna, R. M., Mathur, S., & Yamasaki, N. 1999, *Ap.J.* **519**, 549
- Gehrels, N. 1986, *Ap.J.* **303**, 336
- Green, P. J., et al. 1995, *Ap.J.* **450**, 51
- Green, P. J., & Mathur, S. 1996, *Ap.J.* **462**, 637
- Green, P. J., Aldcroft, T. L., Mathur, S., Wilkes, B. J., & Elvis, M. 2001, *Ap.J.* **558**, 109
- Hamann, F., & Ferland, G. J. 1999, *A.R.A.&A.* **37**, 487
- Hewett, P. C., Foltz, C. B., & Chaffee, F. H. 1995, *A.J.* **109**, 1498
- Kaspi, S., Brandt, W. N., & Schneider, D. P. 2000, *A.J.* **119**, 2031 [KBS]
- Kennefick, J. D., de Carvalho, R. R., Djorgovski, S. G., Wilber, M. M., Dickson, E. S., Weir, N., Fayyad, U., & Roden, J. 1995, *A.J.* **110**, 78
- Kennefick, J. D., Djorgovski, S. G., & de Carvalho, R. R. 1995, *A.J.* **110**, 2553
- Kraft, R. P., Burrows, D. N., & Nousek, J. A. 1991, *Ap.J.* **374**, 344
- Omont, A., Cox, P., Bertoldi, F., McMahon, R. G., Carilli, C., & Isaak, K. G. 2001, *A.&A.* **374**, 371
- Reeves, J. N., & Turner, M. J. L. 2000, *M.N.R.A.S.* **316**, 234
- Schmidt, M., & Green, R. F. 1983, *Ap.J.* **269**, 352

- Schneider, D. P., Schmidt, M., & Gunn, J. E. 1989, *A.J.* **98**, 1951
- Schneider, D. P. 1999, in After the Dark Ages: When Galaxies were Young, ed. S. Holt, & E. Smith (New York: AIP), 233
- Shull, J. M., & van Steenberg, M. E. 1985, *Ap.J.* **298**, 268
- Storrie-Lombardi, L. J., McMahon, R. G., Irwin, M. J., & Hazard, C. 1996, *Ap.J.* **468**, 121
- Venkatesan, A., Giroux, M. L., & Shull, J. M. 2001, *Ap.J.* , in press [astro-ph/0108168]
- Vignali, C., Comastri, A., Cappi, M., Palumbo, G. G. C., Matsuoka, M., & Kubo, H. 1999, *Ap.J.* **516**, 582
- Vignali, C., Brandt, W. N., Fan, X., Gunn, J. E., Kaspi, S., Schneider, D. P., Strauss, M. A. 2001, *A.J.* **122**, in press [astro-ph/0108001]
- York, D. G., et al. 2000, *A.J.* **120**, 1579
- Zheng, W., et al. 2000, *A.J.* **120**, 1607

Acknowledgments

We gratefully acknowledge the financial support of *Chandra* X-ray Center grant G01-2100X (CV, WNB, DPS), the Alfred P. Sloan Foundation (WNB), NSF grant PHY00-70928 and a Frank and Peggy Taplin Fellowship (XF), NASA LTSA grant NAG5-8107 (SK), NSF grant AST99-00703 (DPS), and NSF AST00-71091 (MAS). CV also acknowledges partial support from the Italian Space Agency, under the contract ASI 00/IR/103/AS, and from the Ministry for University and Research (MURST) under grant Cofin-00-02-36.